

A MEDIAN-FILTER-BASED FRAMEWORK FOR INTERFACE OPTIMAL DESIGN PROBLEMS*

SIHAO CHENG[†], ZIMING SHAO[‡], AND DONG WANG[§]

Abstract. We present a robust and efficient numerical framework based on a median filter scheme for solving a broad class of interface-related optimization problems, from image segmentation to topology optimization. A key innovation of our work is the extension of the binary scheme into a continuous level-set scheme via a weighted quantile interpretation. Unlike traditional binary iterative convolution-thresholding method (ICTM), this continuous median filter scheme effectively overcomes the pinning effect caused by spatial discretization, achieving accurate interface evolution even with small time steps. We also provide a rigorous theoretical analysis, proving the unconditional energy stability of the iterative scheme. Furthermore, we prove that for a wide class of data fidelity terms, the convex relaxation inherently enforces a binary solution, justifying the effectiveness of the method without explicit penalization. Numerical experiments on the Chan–Vese model, the local intensity fitting (LIF) model, and topology optimization in Stokes flow demonstrate that the proposed efficient continuous framework effectively eliminates the pinning effect, guarantees unconditional energy stability, and accurately converges to binary solutions.

Key words. interface optimal design, median filter, level-set method, threshold dynamics, topology optimization

MSC codes. 65K10, 65M12, 49Q10, 68U10

1. Introduction. Interface optimal design problems constitute a fundamental class of challenges in computational mathematics, permeating diverse fields ranging from computer vision to fluid mechanics. Prominent examples include the segmentation of complex structures in medical imaging [29, 8, 24], the tracking of immiscible multiphase fluid interfaces in hydrodynamics [20, 31, 21], and the optimal distribution of materials in topology optimization [4, 3, 1, 37]. In these variational problems, the primary objective is to determine an optimal partition of a bounded domain Ω into distinct sub-regions, such as separating foreground from background or distinguishing solids from fluids, in order to minimize a specific, often non-convex energy functional. However, the numerical treatment of these problems is always difficult. The challenges stem not only from the geometric complexity of the interfaces, which may exhibit singularities, but also from the topological changes that occur naturally during the optimization process, such as merging and splitting [12, 11, 34]. Consequently, developing numerical algorithms that are both computationally efficient and mathematically stable, while robustly handling these geometric evolutions, remains a significant and active area of research.

Traditionally, interface evolution modeling uses the level set method [31] and

*This work is partially supported by the National Natural Science Foundation of China (Grant No. 12422116), Guangdong Basic and Applied Basic Research Foundation (Grant No. 2023A1515012199), Shenzhen Science and Technology Innovation Program (Grant Nos. JCYJ20220530143803007, RCYX20221008092843046), and Hetao Shenzhen-Hong Kong Science and Technology Innovation Cooperation Zone Project (No. HZQSW-S-KCCYB-2024016).

[†]School of Science and Engineering, The Chinese University of Hong Kong (Shenzhen), Shenzhen, Guangdong 518172, China (sihaocheng@link.cuhk.edu.cn).

[‡]School of Science and Engineering, The Chinese University of Hong Kong (Shenzhen), Shenzhen, Guangdong 518172, China (zimingshao@link.cuhk.edu.cn).

[§]School of Science and Engineering, The Chinese University of Hong Kong (Shenzhen), Shenzhen, Guangdong 518172, China & Shenzhen International Center for Industrial and Applied Mathematics, Shenzhen Research Institute of Big Data, Guangdong 518172, China & Shenzhen Loop Area Institute, Guangdong 518048, China (wangdong@cuhk.edu.cn).

the phase field method [6, 7, 13]. While these methods have achieved great success in naturally handling complex topological changes, they often encounter significant computational and numerical challenges. For example, the level set method often requires frequent re-initialization to maintain the properties of the signed distance function, which leads to high computational costs [19]. Similarly, the phase field method is governed by nonlinear high-order partial differential equations that depend on a small interface width parameter, and resolving this thin interface requires high grid resolution. Therefore, explicit schemes suffer from severe restrictions of the CFL stability condition [10], while implicit schemes, though more stable, require solving large nonlinear algebraic systems at each step, incurring high computational costs [14, 25].

To alleviate the numerical problems associated with these partial differential equations, Merriman, Bence, and Osher introduced the threshold dynamics method to simulate the mean curvature flow, also known as the MBO method, as an effective alternative [33, 27]. By alternating between diffusion and thresholding steps, the MBO method allows for unconditional stability in time. However, this efficiency comes at the cost of accuracy. MBO schemes typically suffer from the well-known pinning effect, where the interface fails to move if the time step is chosen too small relative to the spatial grid size, leading to superficial convergence or loss of geometric details [16]. This limitation often requires a delicate balance between spatial and temporal discretization, restricting its applicability in high-precision simulations.

In this paper, we propose a generalized median-filter-based framework for solving interface-related optimization problems, inspired by its application to mean curvature flow [15]. While drawing on the efficiency of threshold dynamics, our method differs fundamentally from the traditional binary scheme. By utilizing a weighted quantile interpretation of the heat kernel convolution, we extend the discrete thresholding step into a continuous level-set update scheme. This innovation effectively eliminates the pinning effect associated with spatial discretization, while retaining the unconditional energy stability and the computational efficiency of the original MBO method. In addition, we theoretically establish that, for a wide class of data fidelity terms, the proposed convex relaxation naturally enforces a binary solution, thereby recovering a clear interface without the need for explicit penalty terms. Furthermore, we demonstrate that this framework is not limited to mean curvature flow, but can be rigorously applied to minimize general energy functionals that contain complex data fidelity terms and physical constraints, such as those governed by the Stokes equations.

The rest of this paper is organized as follows. In Section 2, we introduce the mathematical formulation of the interface-related optimization problem and define the associated energy functional in the space of functions of bounded variation. In Section 3, we derive the proposed continuous median filter scheme. By utilizing a weighted quantile interpretation of the heat kernel convolution, this method effectively overcomes the pinning effect inherent in traditional threshold dynamics. Section 4 is dedicated to the rigorous theoretical analysis of the framework. We first prove that for generic data configurations, the convex relaxation automatically enforces a binary solution, ensuring the recovery of sharp interfaces, and then establish the unconditional energy stability of the iterative scheme. Section 5 validates the versatility and robustness of the algorithm through extensive numerical experiments, ranging from image segmentation models, such as the Chan-Vese model and the local intensity fitting (LIF) model, to topology optimization in Stokes flow. Finally, concluding remarks are given in Section 6.

2. Mathematical Model. In this section, we introduce a mathematical model for a class of interface-related optimization problems. The objective is to find an optimal partition of a bounded domain $\Omega \subset \mathbb{R}^2$ and the corresponding optimal parameters that characterize the sub-regions. To ensure the well-posedness of the problem, throughout this paper we assume that Ω is an open, bounded subset with a Lipschitz boundary.

Let $\Omega_1 \subset \Omega$ represent the region of interest (e.g., the foreground in image segmentation or the fluid region in Stokes flow), and let $\Omega_2 = \Omega \setminus \Omega_1$ be the background. Since we are dealing with the geometry of interfaces, the natural mathematical framework is the space of functions of bounded variation, denoted by $BV(\Omega)$. We represent the partition using the characteristic function $u = \mathbb{1}_{\Omega_1}$. Consequently, we define the admissible set for our binary partition variable as follows.

$$(2.1) \quad BV(\Omega; \{0, 1\}) := \{u \in BV(\Omega) : u(\mathbf{x}) \in \{0, 1\}\}.$$

Our goal is to find the optimal function $u \in BV(\Omega; \{0, 1\})$ and the associated parameters \mathbf{c} by minimizing an energy functional. This functional is composed of a fidelity term, which measures the discrepancy between the data and the model parameters within each region, and a geometric regularization term that penalizes the complexity of the interface. We formulate the general energy functional as follows:

$$(2.2) \quad E(u, \mathbf{c}) = \int_{\Omega} u(\mathbf{x}) F_1(\mathbf{x}, \mathbf{c}) \, d\mathbf{x} + \int_{\Omega} (1 - u(\mathbf{x})) F_2(\mathbf{x}, \mathbf{c}) \, d\mathbf{x} + \lambda \text{Per}(\Omega_1).$$

Here, \mathbf{c} represents a vector of parameters (e.g., the average intensity in image segmentation [9] or the velocity fields in Stokes flow [5]) that, together with the function u , completely parameterize the energy functional. The fidelity functions F_1, F_2 measure the cost in each region. We assume that for any fixed \mathbf{c} , $F_1(\cdot, \mathbf{c})$ and $F_2(\cdot, \mathbf{c})$ belong to $L^\infty(\Omega)$, ensuring that the data fidelity terms are finite. The term $\text{Per}(\Omega_1)$ denotes the perimeter of the interface and, weighted by a parameter $\lambda > 0$, penalizes the complexity of the interface to ensure smoothness.

3. Derivation of the Algorithm. In this section, we present our efficient median filter scheme to minimize the energy functional defined in (2.2).

3.1. Approximation of the Perimeter via Heat Kernel. Direct minimization of the energy functional in (2.2) is computationally challenging due to its non-differentiability. To overcome this, we adopt an approximation of the perimeter functional based on the heat kernel.

According to [28], we can approximate the boundary perimeter using the short-time heat content energy:

$$(3.1) \quad \text{Per}(\Omega_1) \approx \mathcal{P}_\tau(u) := \sqrt{\frac{\pi}{\tau}} \int_{\Omega} (1 - u)(\mathbf{x}) (G_\tau * u)(\mathbf{x}) \, d\mathbf{x},$$

where $\tau > 0$ is a small time-scale parameter, and G_τ is the Gaussian kernel (heat kernel) with variance 2τ :

$$(3.2) \quad G_\tau(\mathbf{x}) = \frac{1}{4\pi\tau} \exp\left(-\frac{|\mathbf{x}|^2}{4\tau}\right).$$

As $\tau \rightarrow 0$, this energy $\mathcal{P}_\tau(u)$ converges to the perimeter of Ω_1 in the sense of Γ -convergence. Substituting (3.1) into (2.2), we obtain the approximated energy func-

tional E_τ .

(3.3)

$$E_\tau(u, \mathbf{c}) = \int_{\Omega} u(\mathbf{x})F_1(\mathbf{x}, \mathbf{c}) + (1-u(\mathbf{x}))F_2(\mathbf{x}, \mathbf{c}) \, d\mathbf{x} + \lambda \sqrt{\frac{\pi}{\tau}} \int_{\Omega} (1-u)(\mathbf{x}) (G_\tau * u)(\mathbf{x}) \, d\mathbf{x}.$$

This transformation allows us to handle the geometric regularization effectively using algebraic operations involving convolutions.

3.2. Threshold Dynamics for Characteristic Functions. To minimize the energy functional (3.3), we adopt a coordinate descent strategy [38]. This iterative process involves two main steps:

1. **Update the parameters:** Fix the partition u and update the region parameters \mathbf{c} (e.g., computing the mean intensity). This step is standard and minimizes the fidelity term.
2. **Update the partition:** Fix the parameters \mathbf{c} and find the optimal partition u . This is the critical step where the geometric evolution occurs.

In the following derivation, we focus on the second step: minimizing E_τ with respect to u while keeping \mathbf{c} fixed.

To minimize E_τ with respect to u , we employ a linearization technique. Since the term \mathcal{P}_τ is concave, we linearize the convolution term at the current iteration u^k . The variation of the energy with respect to u leads to the following pointwise condition for u^{k+1} . We set $u^{k+1}(\mathbf{x}) = 1$ if the functional derivative is non-positive, and 0 otherwise. Specifically, $u^{k+1}(\mathbf{x}) = 1$ if and only if:

$$(3.4) \quad F_1(\mathbf{x}) - F_2(\mathbf{x}) + \lambda \sqrt{\frac{\pi}{\tau}} (1 - 2(G_\tau * u^k)(\mathbf{x})) \leq 0.$$

Rearranging the terms, we obtain the threshold dynamics updating rule:

$$(3.5) \quad u^{k+1}(\mathbf{x}) = \mathbb{1}_{\{(G_\tau * u^k)(\mathbf{x}) \geq \frac{1}{2} + \frac{\sqrt{\tau}}{2\lambda\sqrt{\pi}}(F_1(\mathbf{x}) - F_2(\mathbf{x}))\}}(\mathbf{x}).$$

3.3. Median Filter for Level Set Functions. While the threshold dynamics scheme derived in Section 3.2 effectively minimizes the energy for binary functions, achieving sub-grid accuracy often requires a level-set formulation. In this subsection, we extend the binary scheme to continuous functions following the framework in [18].

Let \mathcal{S}_τ denote the operator defined by the update rule (3.5) for a binary characteristic function u . A crucial observation is that \mathcal{S}_τ satisfies the monotonicity property:

LEMMA 3.1 (Monotonicity). *Let $u, v \in BV(\Omega; \{0, 1\})$ be two binary functions such that $u(\mathbf{x}) \leq v(\mathbf{x})$ for almost every $\mathbf{x} \in \Omega$. Then, the operator \mathcal{S}_τ preserves this order, i.e.,*

$$(3.6) \quad (\mathcal{S}_\tau u)(\mathbf{x}) \leq (\mathcal{S}_\tau v)(\mathbf{x}), \quad \text{for all } \mathbf{x} \in \Omega.$$

Proof. Since the heat kernel G_τ is non-negative, the convolution operation is order-preserving. The assumption $u(\mathbf{x}) \leq v(\mathbf{x})$ for almost every $\mathbf{x} \in \Omega$ implies:

$$(3.7) \quad (G_\tau * u)(\mathbf{x}) = \int_{\Omega} G_\tau(\mathbf{x} - \mathbf{y})u(\mathbf{y}) \, d\mathbf{y} \leq \int_{\Omega} G_\tau(\mathbf{x} - \mathbf{y})v(\mathbf{y}) \, d\mathbf{y} = (G_\tau * v)(\mathbf{x}).$$

Let $T(\mathbf{x}) = \frac{1}{2} + \frac{\sqrt{\tau}}{2\lambda\sqrt{\pi}}(F_1(\mathbf{x}) - F_2(\mathbf{x}))$ be the local threshold. If $(\mathcal{S}_\tau u)(\mathbf{x}) = 1$, it implies $(G_\tau * u)(\mathbf{x}) \geq T(\mathbf{x})$. By the inequality above, we necessarily have $(G_\tau * v)(\mathbf{x}) \geq T(\mathbf{x})$, which implies $(\mathcal{S}_\tau v)(\mathbf{x}) = 1$. Since the functions are binary, this confirms that $\mathcal{S}_\tau u \leq \mathcal{S}_\tau v$. \square

This monotonicity allows us to apply the scheme to a general continuous level-set function ϕ by applying the operator to all its super-level sets simultaneously. For a level set function ϕ^k , its super-level set at level s is defined as $\mathcal{T}_\mu \phi^k = \{\mathbf{x} \in \Omega : \phi^k(\mathbf{x}) \geq \mu\}$. The updated value $\phi^{k+1}(\mathbf{x})$ is determined by the highest level μ for which \mathbf{x} remains inside the set evolved from $\mathcal{T}_\mu \phi^k$.

Mathematically, this leads to the following explicit update formula involving the heat kernel weights:

$$(3.8) \quad \phi^{k+1}(\mathbf{x}) = \sup \left\{ \mu \in [0, 1] : \int_{\{\mathbf{y}: \phi^k(\mathbf{y}) \geq \mu\}} G_\tau(\mathbf{x} - \mathbf{y}) d\mathbf{y} \geq T(\mathbf{x}) \right\}.$$

Here, $T(\mathbf{x}) = \frac{1}{2} + \frac{\sqrt{\tau}}{2\lambda\sqrt{\pi}} (F_1(\mathbf{x}) - F_2(\mathbf{x}))$ is the local threshold term derived in Section 3.2.

The formula (3.8) essentially searches for a weighted quantile of the distribution of ϕ^k in the neighborhood of \mathbf{x} . Specifically, if we treat $G_\tau(\mathbf{x} - \cdot)$ as a probability measure, $\phi^{k+1}(\mathbf{x})$ is the value s such that the cumulative weight of neighbors with values greater than or equal to μ exceeds the threshold $T(\mathbf{x})$.

3.4. Algorithm Description. Based on the quantile interpretation in (3.8), the numerical implementation avoids explicit convolution and instead relies on a local sorting strategy. This corresponds to the ‘‘Median Filter’’ solver.

In the numerical implementation, to enhance computational efficiency, we employ a discretization approximation for the convolution step. Specifically, we restrict the support of the convolution kernel to a discrete set of points equidistant from the center \mathbf{x} (i.e., on a circle of fixed radius $R = \sqrt{2\tau}$).

Due to the radial symmetry of the heat kernel G_τ defined in Section 3.1, its value remains constant along the circle. Consequently, the discrete weights w_j at these sample points are identical, effectively reducing the convolution to a uniform average on the circle. Although this geometric approximation might alter the specific pre-factor derived in Section 3.2, in practice, this constant factor is absorbed into the tunable weight parameter λ and does not affect the variational nature of the model.

Algorithm 3.1 Continuous Median Filter Scheme

- 1: **Input:** Data F_1, F_2 , parameters λ, τ .
 - 2: **Initialization:** Choose a continuous level-set function ϕ^0 .
 - 3: **for** $k = 0$ to K_{max} **do**
 - 4: **Step 1: Update Parameters.**
 - 5: Compute region parameters \mathbf{c}^k based on the current level-set function ϕ^k .
 - 6: **Step 2: Continuous Median Filtering.**
 - 7: For each grid point \mathbf{x} :
 - 8: (a) Calculate the threshold $T(\mathbf{x}) = \frac{1}{2} + \frac{\sqrt{\tau}}{2\lambda\sqrt{\pi}} (F_1(\mathbf{x}) - F_2(\mathbf{x}))$.
 - 9: (b) Update $\phi^{k+1}(\mathbf{x}) = \text{GeneralMedianFilter}(\phi^k, T(\mathbf{x}))$.
 - 10: **Step 3: Check Convergence.**
 - 11: If $\|\phi^{k+1} - \phi^k\| < \epsilon$, break.
 - 12: **end for**
 - 13: **Output:** Final level-set function ϕ^{k+1} .
-

In Step 2(b), the operator $\text{GeneralMedianFilter}(\phi, T)$ represents a class of solvers that evolve the interface according to the mean curvature flow subject to an external force T . In Section 5, we will detail the specific implementations of this operator.

4. Theoretical Analysis. In this section, we establish the theoretical foundations of the proposed algorithm. We first prove the equivalence between the level-set formulation and the original binary characteristic formulation using the coarea formula. Furthermore, we prove the existence and uniqueness of the solution and justify its binary property. Next, we demonstrate the unconditional energy stability of the iterative scheme. Finally, we discuss the consistency of the scheme with the mean curvature flow and analyze its stability properties based on the monotonicity principle established in Lemma 3.1.

4.1. Equivalence of Level-Set and Binary Formulations. In this subsection, we establish the theoretical equivalence between the binary optimization problem introduced in Section 2 and the continuous level-set formulation. To streamline the notation and highlight the role of tunable parameters, we introduce an effective weighting parameter $\tilde{\lambda}$ that absorbs the geometric scaling factors inherent in the heat kernel approximation. We define the effective parameter $\tilde{\lambda}$ as:

$$(4.1) \quad \tilde{\lambda} := \lambda \sqrt{\frac{\pi}{\tau}}.$$

DEFINITION 4.1 (Relaxed Energy Functional). *For any function $\phi \in BV(\Omega; [0, 1])$ and fixed parameter \mathbf{c} , we define the relaxed energy functional $\mathcal{E}_\tau(\phi, \mathbf{c})$ as:*

$$(4.2) \quad \begin{aligned} \mathcal{E}_\tau(\phi, \mathbf{c}) := & \int_{\Omega} \int_{\Omega} G_\tau(\mathbf{x} - \mathbf{y}) |\phi(\mathbf{x}) - \phi(\mathbf{y})| d\mathbf{y} d\mathbf{x} \\ & + \frac{2}{\tilde{\lambda}} \int_{\Omega} \left[\phi(\mathbf{x}) F_1(\mathbf{x}, \mathbf{c}) + (1 - \phi(\mathbf{x})) F_2(\mathbf{x}, \mathbf{c}) \right] d\mathbf{x} \end{aligned}$$

Here, the factor 2 accounts for the symmetry in the coarea decomposition, and $\tilde{\lambda}^{-1}$ serves as the relative weight of the data fidelity term.

THEOREM 4.2 (Equivalence via Threshold Decomposition). *Let ϕ^* be a global minimizer of the relaxed energy functional $\mathcal{E}_\tau(\phi, \mathbf{c})$. Then, for almost every threshold level $\mu \in [0, 1]$, the characteristic function $\mathbb{1}_{\mathcal{T}_\mu \phi^*}$ associated with the super-level set*

$$(4.3) \quad \mathcal{T}_\mu \phi^* = \{\mathbf{x} \in \Omega : \phi^*(\mathbf{x}) \geq \mu\}$$

is a global minimizer of the original binary energy functional (3.3).

Proof. Using the generalized coarea identity [15], the interaction term decomposes into the approximate perimeters of the level sets:

$$(4.4) \quad \int_{\Omega} \int_{\Omega} G_\tau(\mathbf{x} - \mathbf{y}) |\phi(\mathbf{x}) - \phi(\mathbf{y})| d\mathbf{y} d\mathbf{x} = 2 \int_0^1 \left[\int_{\Omega} (1 - \mathbb{1}_{\mathcal{T}_\mu \phi}) (G_\tau * \mathbb{1}_{\mathcal{T}_\mu \phi}) d\mathbf{x} \right] d\mu.$$

Using the Cavalieri's Principle for the linear data terms:

$$(4.5) \quad \frac{2}{\tilde{\lambda}} \int_{\Omega} \phi F_1 + (1 - \phi) F_2 d\mathbf{x} = 2 \int_0^1 \left[\frac{1}{\tilde{\lambda}} \int_{\Omega} \mathbb{1}_{\mathcal{T}_\mu \phi} F_1 + (1 - \mathbb{1}_{\mathcal{T}_\mu \phi}) F_2 d\mathbf{x} \right] d\mu.$$

Substituting (4.4) and (4.5) into (4.2), we have:

$$(4.6) \quad \mathcal{E}_\tau(\phi, \mathbf{c}) = \frac{2}{\tilde{\lambda}} \int_0^1 \left[\tilde{\lambda} \int_{\Omega} (1 - \mathbb{1}_{\mathcal{T}_\mu \phi}) (G_\tau * \mathbb{1}_{\mathcal{T}_\mu \phi}) d\mathbf{x} + \int_{\Omega} \mathbb{1}_{\mathcal{T}_\mu \phi} F_1 + (1 - \mathbb{1}_{\mathcal{T}_\mu \phi}) F_2 d\mathbf{x} \right] d\mu.$$

The integrand is exactly the binary energy $E_\tau(\mathbb{1}_{\mathcal{T}_\mu \phi}, \mathbf{c})$. Thus, minimizing \mathcal{E}_τ is equivalent to minimizing E_τ for almost every level μ . \square

While Theorem 4.2 ensures that the super level sets of any minimizer are optimal for the binary problem, it does not explicitly guarantee that the minimizer ϕ^* itself is binary. In the following, we demonstrate that for generic data, the convex relaxation inherently enforces the binary constraint $\phi \in \{0, 1\}$. This justifies the use of the convex model without requiring explicit penalization terms.

To formalize this, let $X = L^1(\Omega)$, and consider the admissible set:

$$(4.7) \quad \mathcal{K} = \{\phi \in BV(\Omega) : 0 \leq \phi(\mathbf{x}) \leq 1 \text{ a.e., and } |D\phi|(\Omega) \leq C\}.$$

The set \mathcal{K} is uniformly bounded in the $BV(\Omega)$ norm. Since the embedding of $BV(\Omega)$ into $L^1(\Omega)$ is compact [2], any bounded subset of $BV(\Omega)$ is relatively compact in $L^1(\Omega)$. Therefore, \mathcal{K} is relatively compact in $L^1(\Omega)$. Furthermore, since \mathcal{K} is closed in L^1 , it becomes a compact subset of X .

Define the interaction functional $J(\phi) = \int_{\Omega} \int_{\Omega} G_{\tau}(\mathbf{x} - \mathbf{y}) |\phi(\mathbf{x}) - \phi(\mathbf{y})| d\mathbf{y} d\mathbf{x}$. Note that J is convex. The total energy is, up to an additive constant independent of ϕ , a linear perturbation of J by the data field $h(\mathbf{x}) = \frac{2}{\lambda}(F_1(\mathbf{x}) - F_2(\mathbf{x}))$:

$$(4.8) \quad \mathcal{E}_{\tau}(\phi) = J(\phi) + \int_{\Omega} \phi(\mathbf{x}) h(\mathbf{x}) d\mathbf{x}.$$

LEMMA 4.3 (Existence and Uniqueness). *Let X be a Banach space, and let $\mathcal{K} \subset X$ be a compact, convex subset. Let $J : \mathcal{K} \rightarrow \mathbb{R}$ be a lower-bounded lower semicontinuous functional. Consider the perturbed functional $\mathcal{E}_h(\phi) = J(\phi) + \langle h, \phi \rangle$ defined on \mathcal{K} . Then there exists a dense G_{δ} subset \mathcal{G} of X^* such that for every perturbation $h \in \mathcal{G}$, the functional \mathcal{E}_h admits a unique global minimizer ϕ^* in \mathcal{K} .*

Proof. Since \mathcal{K} is a compact convex subset of a Banach space, it is dentable [32]. Consequently, invoking Stegall's Variational Principle [35], there exists a dense G_{δ} set \mathcal{G} in X^* such that for all perturbations $h \in \mathcal{G}$, the functional \mathcal{E}_h attains a strong minimum on \mathcal{K} [22]. Since a strong minimizer is necessarily unique, the global minimizer ϕ^* is unique [26]. \square

THEOREM 4.4 (Generic Binary Enforcement). *Let \mathcal{K} be the compact convex set defined above, and let $\mathcal{E}_{\tau}(\phi) = J(\phi) + \int_{\Omega} \phi(\mathbf{x}) h(\mathbf{x}) d\mathbf{x}$ be the energy functional defined on \mathcal{K} . Then there exists a dense G_{δ} subset \mathcal{G} of $L^{\infty}(\Omega)$ such that for every $h \in \mathcal{G}$, the functional \mathcal{E}_{τ} has a unique minimizer ϕ^* in \mathcal{K} , and ϕ^* is binary, i.e., $\phi^*(\mathbf{x}) \in \{0, 1\}$ almost everywhere.*

Proof. By Lemma 4.3, there exists a dense G_{δ} subset \mathcal{G} of $L^{\infty}(\Omega)$ such that for every $h \in \mathcal{G}$, the functional \mathcal{E}_{τ} has a unique minimizer ϕ^* in \mathcal{K} .

Suppose, for contradiction, that ϕ^* is not binary. Then the set $A = \{\mathbf{x} \in \Omega : 0 < \phi^*(\mathbf{x}) < 1\}$ has positive measure. By Theorem 4.2, for almost every $\mu \in (0, 1)$, the characteristic function $\psi_{\mu} = \mathbb{1}_{\{\phi^* \geq \mu\}}$ is a global minimizer of the original binary energy. Since the original binary energy and the relaxed energy \mathcal{E}_{τ} coincide on binary functions, ψ_{μ} is also a global minimizer of \mathcal{E}_{τ} . Now, fix any $\mu \in (0, 1)$ such that the above holds. Since ϕ^* takes values in $(0, 1)$ on A , while ψ_{μ} takes only values 0 or 1, we have $\psi_{\mu} \neq \phi^*$. This yields two distinct global minimizers of \mathcal{E}_{τ} , contradicting the uniqueness guaranteed by Lemma 4.3. Therefore, ϕ^* must be binary almost everywhere. \square

4.2. Derivation of the Scheme and Energy Stability. In this subsection, we derive the explicit update rule of our median filter algorithm and strictly prove its unconditional energy stability. The primary challenge lies in the non-local interaction

term involving $|\phi(\mathbf{x}) - \phi(\mathbf{y})|$, which couples the values of the level-set function across the domain. To decouple these interactions and derive an efficient pointwise solver, we adopt the movement limiter approach proposed in [15].

4.2.1. Derivation of the Iterative Scheme. We introduce an auxiliary functional $\mathcal{M}_k(\phi)$ centered on the current iterate ϕ^k , designed to cancel coupling effects in the interaction term.

DEFINITION 4.5 (Movement Limiter). *Let ϕ^k be the solution in iteration k . Define the movement limiter $\mathcal{M}_k(\phi)$ as:*

$$(4.9) \quad \mathcal{M}_k(\phi) = \int_{\Omega} \int_{\Omega} G_{\tau}(\mathbf{x} - \mathbf{y}) (2|\phi(\mathbf{x}) - \phi^k(\mathbf{y})| - |\phi(\mathbf{x}) - \phi(\mathbf{y})| - |\phi^k(\mathbf{x}) - \phi^k(\mathbf{y})|) d\mathbf{y} d\mathbf{x}.$$

By [15], $\mathcal{M}_k(\phi) \geq 0$ for all ϕ , and $\mathcal{M}_k(\phi^k) = 0$.

Instead of directly minimizing $\mathcal{E}_{\tau}(\phi, \mathbf{c})$, we minimize alternative energy $\mathcal{E}_{\tau}(\phi, \mathbf{c}) + \mathcal{M}_k(\phi)$. The following theorem shows that the global minimizer of this alternative energy is exactly the median filter scheme presented in Algorithm 3.1.

THEOREM 4.6 (Exact Iterative Scheme). *The global minimizer of the alternative problem*

$$(4.10) \quad \phi^{k+1} = \arg \min_{\phi \in BV(\Omega; [0,1])} (\mathcal{E}_{\tau}(\phi, \mathbf{c}) + \mathcal{M}_k(\phi))$$

is given explicitly by the weighted quantile formula (3.8).

Proof. First, we simplify the alternative energy. Substituting (4.2) and (4.9) into (4.10), the coupled terms cancel exactly. Discarding terms independent of ϕ (which do not affect the minimization), the problem reduces to:

$$(4.11) \quad \phi^{k+1} = \arg \min_{\phi} \left[2 \int_{\Omega} \int_{\Omega} G_{\tau}(\mathbf{x} - \mathbf{y}) |\phi(\mathbf{x}) - \phi^k(\mathbf{y})| d\mathbf{y} d\mathbf{x} + \frac{2}{\lambda} \int_{\Omega} (\phi F_1 + (1 - \phi) F_2) d\mathbf{x} \right].$$

Dividing by 2, we observe that the integrand does not contain any spatial derivatives of ϕ . Thus, the global minimization decouples into independent pointwise minimization problems. For each $\mathbf{x} \in \Omega$, we find the value $\xi = \phi^{k+1}(\mathbf{x}) \in [0, 1]$ that minimizes the local potential $J_{\mathbf{x}}(\xi)$:

$$(4.12) \quad J_{\mathbf{x}}(\xi) = \int_{\Omega} G_{\tau}(\mathbf{x} - \mathbf{y}) |\xi - \phi^k(\mathbf{y})| d\mathbf{y} + \frac{1}{\lambda} (\xi F_1(\mathbf{x}) + (1 - \xi) F_2(\mathbf{x})).$$

Since $J_{\mathbf{x}}(\xi)$ is a convex function of ξ , the optimal value is determined by the first-order optimality condition. We examine the derivative with respect to ξ (using the sub-gradient for the absolute value):

$$(4.13) \quad \frac{dJ_{\mathbf{x}}}{d\xi} = \int_{\Omega} G_{\tau}(\mathbf{x} - \mathbf{y}) \cdot \text{sgn}(\xi - \phi^k(\mathbf{y})) d\mathbf{y} + \frac{1}{\lambda} (F_1(\mathbf{x}) - F_2(\mathbf{x})) = 0.$$

Using the normalization condition for G_{τ} and decomposing the sign function integral into regions where $\phi^k < \xi$ and $\phi^k > \xi$, we have:

$$(4.14) \quad \int_{\Omega} G_{\tau}(\mathbf{x} - \mathbf{y}) \cdot \text{sgn}(\xi - \phi^k(\mathbf{y})) d\mathbf{y} = 1 - 2 \int_{\{\mathbf{y}: \phi^k(\mathbf{y}) > \xi\}} G_{\tau}(\mathbf{x} - \mathbf{y}) d\mathbf{y}.$$

Substituting this back into the optimality condition:

$$(4.15) \quad 1 - 2 \int_{\{\mathbf{y}: \phi^k(\mathbf{y}) > \xi\}} G_\tau(\mathbf{x} - \mathbf{y}) d\mathbf{y} + \frac{1}{\lambda}(F_1 - F_2) = 0.$$

Rearranging the terms yields the threshold condition:

$$(4.16) \quad \int_{\{\mathbf{y}: \phi^k(\mathbf{y}) > \xi\}} G_\tau(\mathbf{x} - \mathbf{y}) d\mathbf{y} = T(\mathbf{x}).$$

Since the left-hand side is a monotonically decreasing function of ξ (the super-level set shrinks as the level ξ increases), the optimal solution corresponds to the largest level μ that satisfies the inequality version of (4.16). This is precisely the median filter formula (3.8). \square

4.2.2. Total Energy Stability. We now prove that the proposed algorithm, which alternates between updating the parameters \mathbf{c} and the level-set function ϕ , guarantees the monotonic decay of the total energy.

THEOREM 4.7 (Unconditional Stability). *Let $\{(\phi^k, \mathbf{c}^k)\}$ be the sequence generated by the alternating iterative algorithm. Then, the total energy is non-increasing:*

$$(4.17) \quad \mathcal{E}_\tau(\phi^{k+1}, \mathbf{c}^{k+1}) \leq \mathcal{E}_\tau(\phi^k, \mathbf{c}^k).$$

Proof. First, the parameters are updated to minimize the energy with fixed ϕ^k :

$$\mathbf{c}^{k+1} = \arg \min_{\mathbf{c}} \mathcal{E}(\phi^k, \mathbf{c}).$$

By definition, this implies:

$$(4.18) \quad \mathcal{E}_\tau(\phi^k, \mathbf{c}^{k+1}) \leq \mathcal{E}_\tau(\phi^k, \mathbf{c}^k).$$

Next, ϕ is updated using the scheme (3.8). Since ϕ^{k+1} minimizes the alternative energy $\mathcal{E}_\tau(\cdot, \mathbf{c}^{k+1}) + \mathcal{M}_k(\cdot)$, we have:

$$\begin{aligned} \mathcal{E}_\tau(\phi^{k+1}, \mathbf{c}^{k+1}) &\leq \mathcal{E}_\tau(\phi^{k+1}, \mathbf{c}^{k+1}) + \mathcal{M}_k(\phi^{k+1}) && \text{(Non-negativity of } \mathcal{M}_k) \\ &\leq \mathcal{E}_\tau(\phi^k, \mathbf{c}^{k+1}) + \mathcal{M}_k(\phi^k) && \text{(Minimality of } \phi^{k+1}) \\ &= \mathcal{E}_\tau(\phi^k, \mathbf{c}^{k+1}). && \text{(Contact property } \mathcal{M}_k(\phi^k) = 0) \end{aligned}$$

Combining the inequalities from both steps:

$$(4.19) \quad \mathcal{E}_\tau(\phi^{k+1}, \mathbf{c}^{k+1}) \leq \mathcal{E}_\tau(\phi^k, \mathbf{c}^{k+1}) \leq \mathcal{E}_\tau(\phi^k, \mathbf{c}^k).$$

Thus, the algorithm is unconditionally energy stable. \square

5. Numerical Experiments. In this section, we present several numerical experiments to validate the theoretical properties and practical performance of the proposed median-filter-based framework. Our algorithm is designed as a continuous threshold dynamics scheme: it effectively integrates the numerical stability of traditional threshold dynamics with the geometric continuity of level-set representations. This unique combination allows for robust interface evolution even under challenging numerical settings.

5.1. Numerical Implementation via Weighted Quantile Filter. The core of our numerical framework lies in the efficient evaluation of the convolution thresholding step. Unlike the traditional binary MBO scheme, which relies on direct convolution thresholding that leads to the pinning effect, our approach implements the update via a weighted quantile filter acting on the continuous level-set function ϕ [30].

For a discretized domain, the Gaussian kernel G_τ is approximated by a discrete mask W with weights $\{w_j\}_{j=1}^M$. The update for the level-set function $\phi^{k+1}(\mathbf{x})$ at each grid point \mathbf{x} is computed as follows:

1. **Neighbor Evaluation:** We sample the values of the current level-set function ϕ^k within the neighborhood of \mathbf{x} . To maintain sub-grid accuracy, these values $\{\phi^k(\mathbf{x} + \mathbf{y}_j)\}_{j=1}^M$ can be evaluated using bilinear interpolation [36].
2. **Sorting:** The sampled values are sorted in descending order, denoted as $v_{(1)} \geq v_{(2)} \geq \dots \geq v_{(M)}$.
3. **Quantile Selection:** We calculate the cumulative weights of the sorted neighbors. The new value $\phi^{k+1}(\mathbf{x})$ is determined by selecting the value $v_{(m)}$ that corresponds to the specific quantile required by (3.8).

This procedure, summarized in Algorithm 5.1, allows the level-set function to take values from a continuous range rather than being restricted to a binary set. By selecting the update value from the sorted continuous neighbors, the interface can move by arbitrary sub-grid distances, thereby effectively eliminating the pinning effect associated with spatial discretization.

Algorithm 5.1 Continuous Median Filter Scheme via Weighted Quantile

- 1: **Input:** Current level-set function ϕ^k , time step τ , kernel weights $\{w_j\}_{j=1}^M$.
 - 2: **Initialization:** Generate the discrete mask $W = \{w_j\}$ approximating G_τ .
 - 3: **for** each grid point \mathbf{x} in the domain **do**
 - 4: Sample neighbors $\{\phi^k(\mathbf{x} + \mathbf{y}_j)\}_{j=1}^M$ using bilinear interpolation.
 - 5: Sort the sampled values in descending order: $v_{(1)} \geq v_{(2)} \geq \dots \geq v_{(M)}$.
 - 6: Compute cumulative weights $S_m = \sum_{l=1}^m w_{(l)}$, where $w_{(l)}$ is the weight for $v_{(l)}$.
 - 7: Find the first index m^* satisfying $S_{m^*} \geq T(\mathbf{x})$.
 - 8: Set $\phi^{k+1}(\mathbf{x}) = v_{(m^*)}$.
 - 9: **end for**
 - 10: **Output:** Updated level-set function ϕ^{k+1} .
-

5.2. Continuity Verification via the Chan-Vese Model. We begin by applying our framework to the classical Chan-Vese (CV) model for bi-phasic image segmentation [8]. This experiment aims to demonstrate that our continuous formulation successfully resolves the discretization issues inherent in classical binary thresholding schemes.

5.2.1. Model Formulation and Parameter Update. Consider a grayscale image $I : \Omega \rightarrow \mathbb{R}$. The CV model minimizes an energy functional balancing region-based fidelity and interface length. Within our general framework, the fidelity functions are:

$$(5.1) \quad F_1(\mathbf{x}, \mathbf{c}) = |I(\mathbf{x}) - c_1|^2, \quad F_2(\mathbf{x}, \mathbf{c}) = |I(\mathbf{x}) - c_2|^2.$$

where $\mathbf{c} = (c_1, c_2)$ are the region constants. By fixing the partition ϕ^k , the optimal parameters c_1^{k+1} and c_2^{k+1} are updated via the following recursive mean-value formulas:

$$(5.2) \quad c_1^{k+1} = \frac{\int_{\Omega} \phi^k(\mathbf{x}) I(\mathbf{x}) d\mathbf{x}}{\int_{\Omega} \phi^k(\mathbf{x}) d\mathbf{x}}, \quad c_2^{k+1} = \frac{\int_{\Omega} (1 - \phi^k(\mathbf{x})) I(\mathbf{x}) d\mathbf{x}}{\int_{\Omega} (1 - \phi^k(\mathbf{x})) d\mathbf{x}}.$$

5.2.2. Comparison of Continuity: Small τ Behavior. One of the primary motivations for adopting the continuous level-set formulation (the median filter scheme) is to overcome the limitations of binary characteristic function formulation (the threshold dynamics scheme) on discrete grids. In the binary setting, where $u \in \{0, 1\}$, the evolution of the interface is governed by a simple thresholding rule (3.5). When the time-scale parameter τ is chosen to be very small, the interface often fails to move because the local forcing term $T(\mathbf{x})$ is insufficient to “flip” the binary value of a pixel, leading to the pinning effect.

In contrast, our median filter approach evolves a continuous level-set function $\phi \in [0, 1]$ using the weighted quantile update (3.8). Because ϕ can take values between 0 and 1, the scheme effectively interpolates the interface position between grid points. This “continuity” allows the level-set function to undergo infinitesimal changes at each iteration, even when τ is extremely small.

Figure 1 visually demonstrates this phenomenon. The experiment involves segmenting a noisy image containing multiple geometric shapes corrupted by Gaussian noise. For all simulations presented in this figure, the parameter is fixed at $\tilde{\lambda} = 0.6$. The figure compares the segmentation results of the traditional binary threshold dynamics (TD) scheme and our proposed median filter (MF) algorithm with varying time steps τ . As τ decreases, the TD method exhibits increasing instability: it fails to handle topological changes (splitting) at intermediate steps and eventually freezes due to the pinning effect, failing to evolve from the initial contour (as seen at $\tau = 10^{-4}$). In contrast, our MF method maintains a smooth and accurate interface evolution even for the smallest τ value, effectively verifying the “continuity” property of our level-set formulation.

5.3. Interface Sharpness Verification via the Chan-Vese Model. In this section, we conduct numerical experiments to validate the theoretical assertions regarding the interface sharpening property. The primary objective is to demonstrate that the proposed median filter scheme effectively drives the interface from a continuous initialization to a sharp profile and converges to the geometric steady state predicted by the analysis in Theorem 4.4.

The numerical validation is performed with a fixed time step $\tau = 10^{-3}$ and the parameter $\tilde{\lambda} = 0.6$. The computational domain Ω is discretized on a uniform grid. The initialization is chosen as a regularized signed distance function with a conical profile. Specifically, it is normalized to have a maximum value of $\phi = 1$ at the domain center and linearly decays to $\phi = 0$ at the domain corners. We observe its morphological evolution and the recovery of sharpness as it approaches the stationary state.

Figure 2 presents a comprehensive visualization of the interface evolution, organized into two perspectives to verify the theoretical predictions. The top row (3D views) displays the morphological evolution of the interface level set function ϕ , capturing the spatial transition from the conical initialization to the sharp, cylindrical steady state. Concurrently, the bottom row (histograms) illustrates the statistical evolution of the function values. As time progresses, the distribution shifts from a broad spread across the interval $[0, 1]$ to a binary concentration at the endpoints $\{0, 1\}$, providing quantitative evidence of the sharpening effect and the suppression of numerical diffusion.

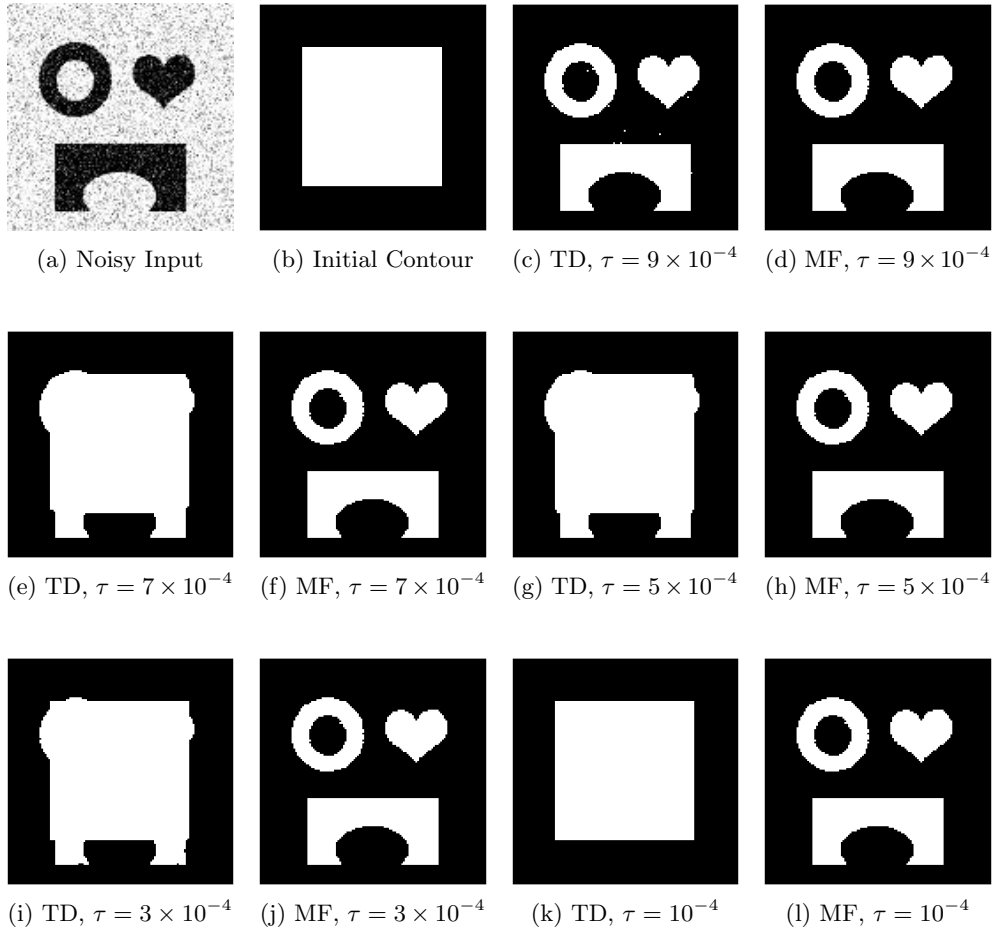


Fig. 1: Visual comparison of segmentation results on a noisy image with different time steps τ . The parameter is set to $\tilde{\lambda} = 0.6$. (a) The noisy input image. (b) The initial square contour. (c)–(l) Comparison between the traditional threshold dynamics (TD) method and the proposed median filter (MF) scheme with decreasing time steps $\tau \in \{9, 7, 5, 3, 1\} \times 10^{-4}$. It can be observed that the MF scheme (d, f, h, j, l) consistently achieves accurate segmentation regardless of the time step size. In contrast, the TD method demonstrates significant instability: at intermediate time steps (e, g, i), it fails to handle topological changes (splitting); and at a small time step (k), it suffers from the severe pinning effect, where the contour fails to evolve from the initialization (compare k with b).

5.3.1. High-Order Implementation via Quadratic Interpolation. To improve geometric accuracy, we propose the following quadratic interpolation algorithm, which effectively captures the local geometric features of the image.

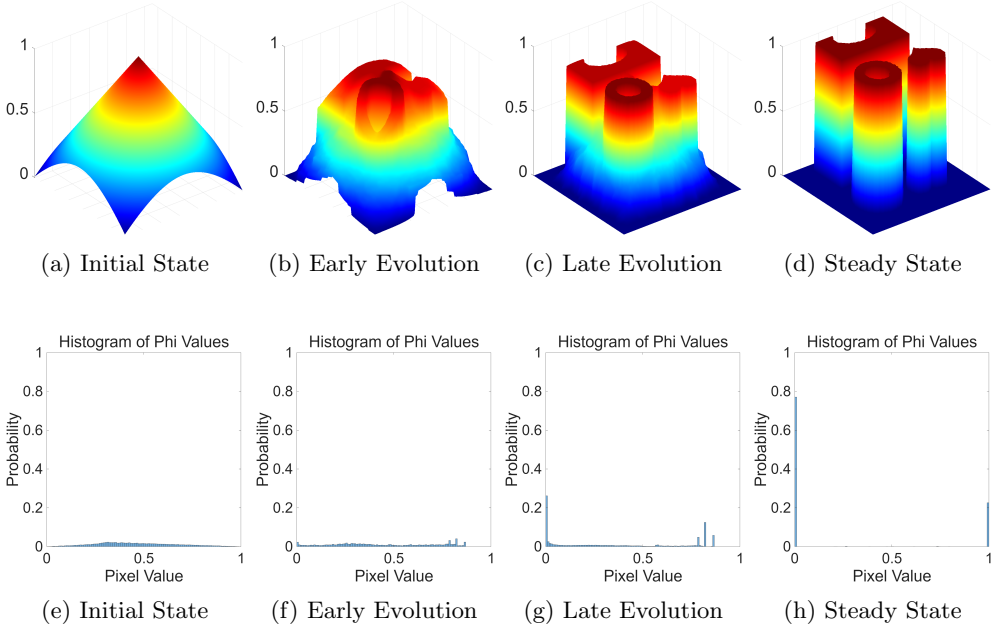


Fig. 2: Visual verification of sharpness. Top row: 3D evolution of the interface level set function ϕ showing the sharpening process. Bottom row: Corresponding histograms of pixel values showing the transition from a continuous distribution to a binary state. The columns represent the progression from initialization (left) to the final geometric steady state (right).

Algorithm 5.2 Continuous Median Filter Scheme via Quadratic Interpolation

- 1: **Input:** Current level-set function ϕ^k , time step τ .
 - 2: **for** each grid point \mathbf{x} in the domain **do**
 - 3: Sample neighbors $\{\phi^k(\mathbf{x} + \mathbf{y}_j)\}_{j=1}^M$ on a circle with center \mathbf{x} and radius τ .
 - 4: Construct local quadratic polynomial $\mathcal{P}(\theta)$ approximate values on the circle.
 - 5: Find ϕ^* such that $|\{\theta \in [0, 2\pi) : \mathcal{P}(\theta) < \phi^*\}| = 2\pi T(\mathbf{x})$.
 - 6: Set $\phi^{k+1}(\mathbf{x}) = \phi^*$.
 - 7: **end for**
 - 8: **Output:** Updated level-set function ϕ^{k+1} .
-

Remark 5.1. In practice, to achieve sub-grid accuracy, we discretize the neighborhood boundary into $M = 8$ equidistant sampling points. These nodes partition the domain into 4 non-overlapping segments. On each segment $i \in \{1, \dots, 4\}$, the local level-set function is approximated by a quadratic polynomial $\mathcal{P}_i(\theta) = c_{2,i}\theta^2 + c_{1,i}\theta + c_{0,i}$, uniquely determined by the nodal values at the two endpoints and one midpoint.

While the Chan-Vese model performs well on images with distinct, homogeneous regions, it relies on the assumption that the intensity within each phase is approximately piecewise constant. This assumption fails in the presence of intensity inhomogeneity (e.g., uneven illumination), where a global fitting term is insufficient. This limitation motivates the need for more sophisticated energy functionals. In the next

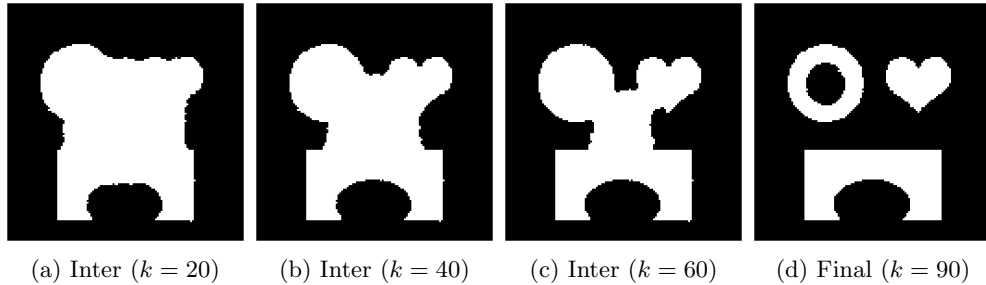


Fig. 3: The simulation is performed with a time step $\tau = 5 \times 10^{-4}$, and the effective parameter $\tilde{\lambda} = 0.6$. The sequence illustrates the robust evolution of the contour, effectively capturing geometric details and handling topological changes, finally converging to a sharp binary solution at iteration $k = 90$.

section, we demonstrate that our median-filter framework is flexible enough to handle such complex scenarios by employing the local intensity fitting (LIF) model.

5.4. Stability Verification via Local Intensity Fitting (LIF). To rigorously test the stability of our algorithm (Theorem 4.7) under more complex energy functionals, we employ the local intensity fitting (LIF) model. Unlike the Chan-Vese model which assumes global constant intensities, the LIF model captures the local intensity information of the image. Specifically, it is designed to deal with intensity inhomogeneity by minimizing the smoothed error between the original image and the local fitting image. This capability is essential for segmenting images with severe intensity inhomogeneity and noise.

5.4.1. Model Formulation and Parameter Update. Consider a grayscale image $I : \Omega \rightarrow \mathbb{R}$. The LIF model minimizes an energy functional that handles intensity inhomogeneities by using local region statistics. The fidelity functional is defined as:

$$(5.3) \quad F_i(\mathbf{y}, \mathbf{c}) = \int_{\Omega} G_{\sigma}(\mathbf{x} - \mathbf{y}) |C_i(\mathbf{x}) - I(\mathbf{y})|^2 d\mathbf{x}, \quad i = 1, 2,$$

where G_{σ} is a Gaussian kernel with variance 2σ , and C_i represents the local intensity means.

By fixing the partition ϕ^k , the optimal local means C_1 and C_2 satisfy the Euler-Lagrange equations and are updated via the following convolution formulas:

$$(5.4) \quad C_1^{k+1}(\mathbf{x}) = \frac{(G_{\sigma} * (\phi^k I))(\mathbf{x})}{(G_{\sigma} * \phi^k)(\mathbf{x})}, \quad C_2^{k+1}(\mathbf{x}) = \frac{(G_{\sigma} * ((1 - \phi^k)I))(\mathbf{x})}{(G_{\sigma} * (1 - \phi^k))(\mathbf{x})}.$$

Here, $*$ denotes the convolution operation.

5.4.2. Validation of Stability: Energy Decay. The validation of the unconditional stability property focuses on the monotonicity of the energy evolution within our median-filter-based framework. Figure 4 presents the segmentation process in an image characterized by severe intensity inhomogeneity, serving as a stress test for the LIF model.

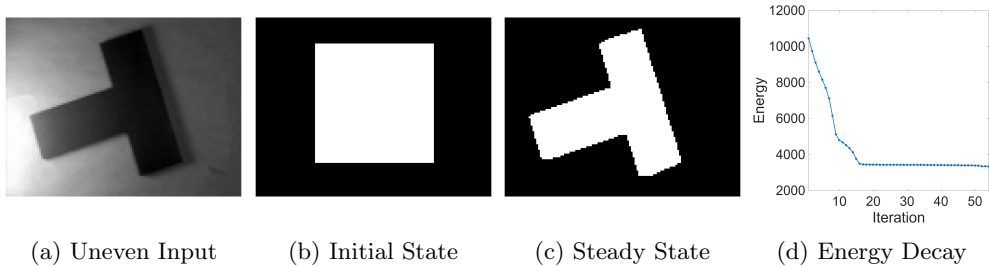


Fig. 4: Numerical verification of the proposed method using the LIF model. (a)–(c) The algorithm successfully overcomes intensity inhomogeneity by utilizing local intensity information to guide the contour. (d) The energy decreases monotonically, empirically confirming the unconditional stability claimed in Theorem 4.7 for the median-filter-based iteration.

Figure 4(a)–(c) illustrate the robustness of the proposed method. The algorithm successfully navigates the complex energy functional to recover the accurate boundary of the object. This numerically verifies that our median filtering scheme effectively approximates the gradient flow of complex energy functionals.

Furthermore, the corresponding energy curve is plotted in Figure 4(d). As predicted by the stability assertion in Theorem 4.7, the total energy exhibits a monotonic decay throughout the iterations, stabilizing rapidly. This result demonstrates that the proposed framework maintains its energy-dissipation property even when applied to complex functionals involving local convolutions, providing a numerical validation of the theoretical stability analysis.

While this subsection focused on image segmentation, the mathematical structure of the problem is entirely consistent with interface problems in physics. In the following subsection, we demonstrate the generality of our framework by extending it to topology optimization in fluid dynamics.

5.5. Stability Verification via Physics Constraints: Topology Optimization in Stokes Flow. To rigorously extend the validation of Theorem 4.7 to physics-driven problems, we apply our framework to topology optimization in fluid dynamics. Unlike the image segmentation task where the data is static, this problem involves a state equation constraint governed by the Stokes equations. This serves as a stress test for the algorithm’s stability when the driving force is dynamically updated by solving a partial differential equation at each iteration.

5.5.1. Model Formulation and Force Calculation. We consider the optimal distribution of fluid within a design domain Ω to minimize energy dissipation. The flow is governed by the Stokes equations with a Brinkman penalization term to model the solid structures. The state variables velocity \mathbf{v} and pressure p satisfy:

$$(5.5) \quad \begin{aligned} -\nabla \cdot (\eta D(\mathbf{v})) + \alpha(\phi) \mathbf{v} + \nabla p &= \mathbf{f} & \text{in } \Omega, \\ \nabla \cdot \mathbf{v} &= 0 & \text{in } \Omega, \end{aligned}$$

where $D(\mathbf{v})$ is the strain rate tensor and η is the viscosity. The inverse permeability $\alpha(\phi)$ acts as the penalization parameter, defined as $\alpha(\phi) = \bar{\alpha} G_\tau * (1 - \phi)$ to distinguish between fluid and solid regions.

Analogous to the local parameter update in the LIF model, the driving forces F_i for the median filter are derived from the first variation of the energy functional. At each iteration k , given the partition ϕ^k , we solve (5.5) for \mathbf{v}^k and update the force field as:

$$(5.6) \quad F_1^{k+1} = 0, \quad F_2^{k+1} = \frac{1}{2} \bar{\alpha} G_\tau * |\mathbf{v}^k|^2.$$

These force terms F_i are then substituted into the median-filtering scheme to evolve the interface.

5.5.2. Handling of Volume Constraint. While the model formulation above defines the energy minimization framework, a critical step in the numerical implementation is the preservation of the fluid volume. To strictly enforce the global constraint $\int_\Omega \phi \, d\mathbf{x} = V_{target}$ during the optimization process, we employ an augmented Lagrangian approach coupled with a root-finding algorithm.

Mathematically, the volume constraint is incorporated into the energy functional by introducing a Lagrange multiplier Λ . The total energy becomes:

$$(5.7) \quad \mathcal{E}_{total}(\phi, \mathbf{c}, \Lambda) = \mathcal{E}_\tau(\phi, \mathbf{c}) + \Lambda \left(\int_\Omega \phi \, d\mathbf{x} - V_{target} \right).$$

In the context of our median filter scheme (3.8), the inclusion of the linear volume term manifests as a global shift in the threshold level. Specifically, the updating rule is modified to:

$$(5.8) \quad \phi^{k+1}(\mathbf{x}) = \sup \left\{ \mu \in [0, 1] : \int_{\{\mathbf{y}: \phi^k(\mathbf{y}) \geq \mu\}} G_\tau(\mathbf{x} - \mathbf{y}) \, d\mathbf{y} \geq T(\mathbf{x}) + \Lambda^k \right\}.$$

where Λ^k is a scalar offset corresponding to the Lagrange multiplier.

In our numerical implementation, finding the optimal Λ^k that satisfies the volume constraint is equivalent to finding the root of the monotonic function $V(\Lambda) = \int_\Omega \phi^{k+1}(\Lambda) \, d\mathbf{x} - V_{target}$. We solve this efficiently using the bisection method at each iteration. This ensures that the generated partition ϕ^{k+1} strictly satisfies the prescribed volume fraction β , where $V_{target} = \beta|\Omega|$, with a tolerance of 10^{-5} . With the specific handling of constraints established, we now proceed to validate the stability of the proposed framework.

5.5.3. Validation of Stability: Energy Decay. The validation of the unconditional stability property focuses on the monotonicity of the energy evolution for these physics constrained problems. To demonstrate the universality and robustness of our framework, we conduct stress tests on two distinct benchmark examples with different Dirichlet boundary conditions:

1. A ‘‘Flow Contraction’’ problem. As shown in Figure 5(a), fluid enters through the entire left boundary with a height of 1 and is constrained to exit through a narrow outlet of height 1/3 located at the center of the right boundary. This setup imposes a severe geometric constraint, challenging the algorithm to form a smooth converging channel while minimizing energy dissipation.
2. A ‘‘Two-Inlet Two-Outlet’’ problem. As illustrated in Figure 6(a), the domain features two separate inlets on the left boundary and two separate outlets on the right. Each opening has a height of 1/6, symmetrically distributed. This configuration serves as a stress test to verify whether the algorithm will preserve the topological separation of the flow paths or merge them to minimize resistance, depending on the energy functional.

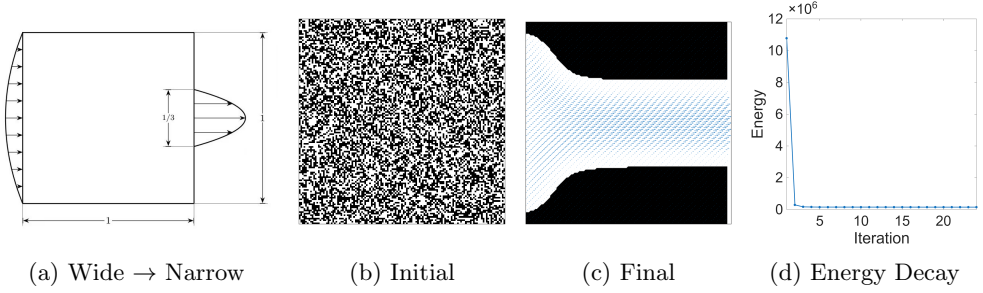


Fig. 5: Numerical verification of the proposed framework on the Flow Contraction problem. (a) Domain setup with a full-height inlet transitioning to a restricted outlet of height $1/3$. (b) Initial random state. (c) The algorithm successfully forms a smooth converging channel. (d) The energy curve confirms unconditional stability.

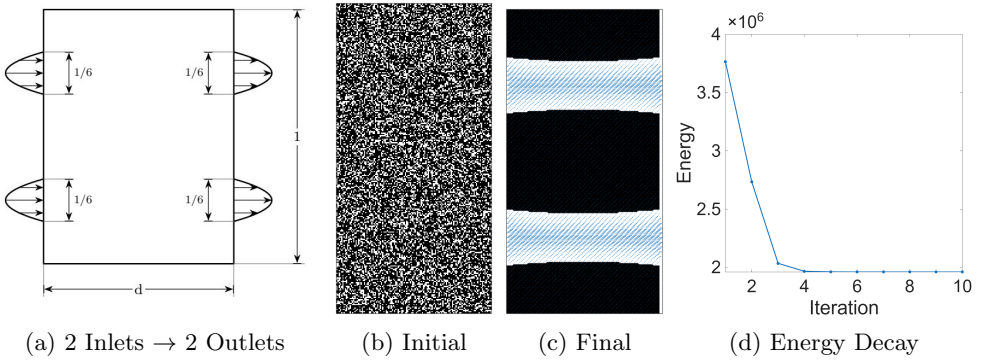


Fig. 6: Numerical verification of the proposed framework on the “Two-Inlet Two-Outlet” problem. (a) Domain setup featuring two separate inlets and outlets, each with a height of $1/6$. (b) Initial random state. (c) The energy curve confirms unconditional stability. (d) The algorithm successfully recovers a double-channel structure.

Figures 5 and 6 present the optimization processes for the “Flow Contraction” problem and the “Two-Inlet Two-Outlet” problem, respectively. To test the robustness of the algorithm against local minima, we initialize both designs with random noise, representing chaotic material distributions.

The visualization of the results illustrates the capability of the proposed method to self-organize from a random state in different geometric settings. In both cases, the algorithm successfully navigates the complex energy functional, where the “force” is implicitly determined by the PDE solution, to recover a smooth channel structure. This numerically verifies that our median filtering scheme effectively approximates the gradient flow even when the energy functional involves global PDE constraints.

Furthermore, the corresponding energy curves are plotted in Figures 5(c) and 6(c). As predicted by the stability assertion in Theorem 4.7, the total energy dissipation exhibits a monotonic decay throughout the iterations for both examples, stabiliz-

ing rapidly. These results collaboratively demonstrate that the proposed framework maintains its energy-dissipation property across different physics-driven applications, providing strong numerical validation of the theoretical stability analysis.

6. Conclusions. In this paper, we have proposed a general and robust numerical framework based on the median filter scheme for solving variational problems with perimeter regularization. By interpreting the median filter as a distinct threshold dynamics solver, we established a rigorous theoretical foundation for the method. Specifically, we proved the unconditional energy stability of the iterative scheme and demonstrated that, for generic data, the proposed convex relaxation naturally enforces a binary solution without the need for explicit penalization terms. A key advantage of our approach is its capability to effectively mitigate the pinning effect, which commonly plagues traditional threshold dynamics methods, without sacrificing computational efficiency.

Extensive numerical experiments have verified the versatility and effectiveness of the proposed framework. We successfully applied the method to two distinct fields: image segmentation (using Chan-Vese and local intensity fitting models) and topology optimization for Stokes flow. The results indicate that our algorithm not only accurately captures complex topological changes and preserves volume constraints but also maintains stability across a wide range of parameters. The seamless integration of the level-set formulation with the median filtering operation provides a simple yet powerful tool for interface related optimization problems.

While our results are encouraging, several avenues for future research remain open. Specifically, the current framework is designed primarily for binary-phase problems; extending the median-filter-based approach to multiphase problems with multiple junctions remains a challenging but worthwhile direction [23]. Furthermore, although we have addressed topology optimization in Stokes flow, applying this method to Navier-Stokes equations or fluid-structure interaction problems would require further investigation into the coupling strategies [17].

REFERENCES

- [1] G. ALLAIRE, F. JOUVE, AND A.-M. TOADER, *Structural optimization using sensitivity analysis and a level-set method*, Journal of Computational Physics, 194 (2004), pp. 363–393, <https://doi.org/10.1016/j.jcp.2003.09.032>.
- [2] L. AMBROSIO, N. FUSCO, AND D. PALLARA, *Functions of Bounded Variation and Free Discontinuity Problems*, Oxford University PressOxford, Mar. 2000, <https://doi.org/10.1093/oso/9780198502456.001.0001>.
- [3] M. P. BENDSØE, *Optimal shape design as a material distribution problem*, Structural Optimization, 1 (1989), pp. 193–202, <https://doi.org/10.1007/BF01650949>.
- [4] M. P. BENDSØE AND O. SIGMUND, *Topology Optimization*, Springer Berlin Heidelberg, Berlin, Heidelberg, 2004, <https://doi.org/10.1007/978-3-662-05086-6>.
- [5] T. BORRVALL AND J. PETERSSON, *Topology optimization of fluids in Stokes flow*, International Journal for Numerical Methods in Fluids, 41 (2003), pp. 77–107, <https://doi.org/10.1002/flid.426>.
- [6] J. W. CAHN AND J. E. HILLIARD, *Free Energy of a Nonuniform System. I. Interfacial Free Energy*, The Journal of Chemical Physics, 28 (1958), pp. 258–267, <https://doi.org/10.1063/1.1744102>.
- [7] J. W. CAHN AND J. E. HILLIARD, *Free Energy of a Nonuniform System. III. Nucleation in a Two-Component Incompressible Fluid*, The Journal of Chemical Physics, 31 (1959), pp. 688–699, <https://doi.org/10.1063/1.1730447>.
- [8] T. CHAN AND L. VESE, *Active contours without edges*, IEEE Transactions on Image Processing, 10 (2001), pp. 266–277, <https://doi.org/10.1109/83.902291>.
- [9] T. F. CHAN, S. ESEDOGLU, AND M. NIKOLOVA, *Algorithms for Finding Global Minimizers of Image Segmentation and Denoising Models*, SIAM Journal on Applied Mathematics, 66

- (2006), pp. 1632–1648, <https://doi.org/10.1137/040615286>.
- [10] L. CHEN AND J. SHEN, *Applications of semi-implicit Fourier-spectral method to phase field equations*, Computer Physics Communications, 108 (1998), pp. 147–158, [https://doi.org/10.1016/S0010-4655\(97\)00115-X](https://doi.org/10.1016/S0010-4655(97)00115-X).
- [11] T. COLDING AND W. MINICOZZI, *Generic mean curvature flow I; generic singularities*, Annals of Mathematics, 175 (2012), pp. 755–833, <https://doi.org/10.4007/annals.2012.175.2.7>.
- [12] K. DECKELNICK, G. DZIUK, AND C. M. ELLIOTT, *Computation of geometric partial differential equations and mean curvature flow*, Acta Numerica, 14 (2005), pp. 139–232, <https://doi.org/10.1017/S0962492904000224>.
- [13] Q. DU AND X. FENG, *The phase field method for geometric moving interfaces and their numerical approximations*, 21 (2020), pp. 425–508, <https://doi.org/10.1016/bs.hna.2019.05.001>.
- [14] E. EREN, B. RUNNELS, AND J. MASON, *Comparison of evolving interfaces, triple points, and quadruple points for discrete and diffuse interface methods*, Computational Materials Science, 213 (2022), p. 111632, <https://doi.org/10.1016/j.commatsci.2022.111632>.
- [15] S. ESEDOĞLU, J. GUO, AND D. LI, *On median filters for motion by mean curvature*, Mathematics of Computation, (2024), <https://doi.org/10.1090/mcom/3940>.
- [16] S. ESEDOĞLU, S. RUUTH, AND R. TSAI, *Diffusion generated motion using signed distance functions*, Journal of Computational Physics, 229 (2010), pp. 1017–1042, <https://doi.org/10.1016/j.jcp.2009.10.002>.
- [17] F. FEPPON, G. ALLAIRE, C. DAPOGNY, AND P. JOLIVET, *Topology optimization of thermal fluid–structure systems using body-fitted meshes and parallel computing*, Journal of Computational Physics, 417 (2020), p. 109574, <https://doi.org/10.1016/j.jcp.2020.109574>.
- [18] J. GUO AND S. ESEDOĞLU, *Median Filters for Anisotropic Wetting / Dewetting Problems*, SIAM Journal on Scientific Computing, 47 (2025), pp. A2012–A2039, <https://doi.org/10.1137/24M1670755>.
- [19] D. HARTMANN, M. MEINKE, AND W. SCHRÖDER, *The constrained reinitialization equation for level set methods*, Journal of Computational Physics, 229 (2010), pp. 1514–1535, <https://doi.org/10.1016/j.jcp.2009.10.042>.
- [20] C. HIRT AND B. NICHOLS, *Volume of fluid (VOF) method for the dynamics of free boundaries*, Journal of Computational Physics, 39 (1981), pp. 201–225, [https://doi.org/10.1016/0021-9991\(81\)90145-5](https://doi.org/10.1016/0021-9991(81)90145-5).
- [21] D. JACQMIN, *Calculation of Two-Phase Navier–Stokes Flows Using Phase-Field Modeling*, Journal of Computational Physics, 155 (1999), pp. 96–127, <https://doi.org/10.1006/jcph.1999.6332>.
- [22] M. LASSONDE, *Asplund Spaces, Stegall Variational Principle and the RNP*, Set-Valued and Variational Analysis, 17 (2009), pp. 183–193, <https://doi.org/10.1007/s11228-009-0111-6>.
- [23] T. LAUX AND T. M. SIMON, *Convergence of the Allen-Cahn Equation to Multiphase Mean Curvature Flow*, Communications on Pure and Applied Mathematics, 71 (2018), pp. 1597–1647, <https://doi.org/10.1002/cpa.21747>.
- [24] C. LI, C.-Y. KAO, J. C. GORE, AND Z. DING, *Implicit Active Contours Driven by Local Binary Fitting Energy*, in 2007 IEEE Conference on Computer Vision and Pattern Recognition, Minneapolis, MN, USA, June 2007, IEEE, pp. 1–7, <https://doi.org/10.1109/CVPR.2007.383014>.
- [25] D. LI, Z. QIAO, AND T. TANG, *Characterizing the stabilization size for semi-implicit fourier-spectral method to phase field equations*, SIAM Journal on Numerical Analysis, 54 (2016), pp. 1653–1681, <https://doi.org/10.1137/140993193>.
- [26] P. D. LOEWEN AND X. WANG, *A Generalized Variational Principle*, Canadian Journal of Mathematics, 53 (2001), pp. 1174–1193, <https://doi.org/10.4153/CJM-2001-044-8>.
- [27] B. MERRIMAN, J. K. BENICE, AND S. J. OSHER, *Motion of Multiple Junctions: A Level Set Approach*, Journal of Computational Physics, 112 (1994), pp. 334–363, <https://doi.org/10.1006/jcph.1994.1105>.
- [28] M. MIRANDA, D. PALLARA, F. PARONETTO, AND M. PREUNKERT, *Short-time heat flow and functions of bounded variation in R^N* , vol. 16, Dec. 2008, pp. 125–145, <https://doi.org/10.5802/afst.1142>.
- [29] D. MUMFORD AND J. SHAH, *Optimal approximations by piecewise smooth functions and associated variational problems*, Communications on Pure and Applied Mathematics, 42 (1989), pp. 577–685, <https://doi.org/10.1002/cpa.3160420503>.
- [30] A. M. OBERMAN, *A convergent monotone difference scheme for motion of level sets by mean curvature*, Numerische Mathematik, 99 (2004), pp. 365–379, <https://doi.org/10.1007/s00211-004-0566-1>.
- [31] S. OSHER AND J. A. SETHIAN, *Fronts propagating with curvature-dependent speed: Algorithms based on Hamilton-Jacobi formulations*, Journal of Computational Physics, 79 (1988),

- pp. 12–49, [https://doi.org/10.1016/0021-9991\(88\)90002-2](https://doi.org/10.1016/0021-9991(88)90002-2).
- [32] M. RIEFFEL, *Dentable subsets of banach spaces, with applications to a radon-nikodym theorem*, in Proc. Conf. Functional Analysis, Thompson Book Co., Washington, DC, 1967, pp. 71–77.
- [33] S. J. RUUTH, B. MERRIMAN, J. XIN, AND S. OSHER, *Diffusion-Generated Motion by Mean Curvature for Filaments*, vol. 11, Dec. 2001, <https://doi.org/10.1007/s00332-001-0404-x>.
- [34] R. SAYE AND J. A. SETHIAN, *A review of level set methods to model interfaces moving under complex physics: Recent challenges and advances*, 21 (2020), pp. 509–554, <https://doi.org/10.1016/bs.hna.2019.07.003>.
- [35] C. STEGALL, *Optimization of functions on certain subsets of Banach spaces*, Mathematische Annalen, 236 (1978), pp. 171–176, <https://doi.org/10.1007/BF01351389>.
- [36] R. TAKEI, *Modern theory of numerical methods for motion by mean curvature*, (2007).
- [37] A. TAKEZAWA, S. NISHIWAKI, AND M. KITAMURA, *Shape and topology optimization based on the phase field method and sensitivity analysis*, Journal of Computational Physics, 229 (2010), pp. 2697–2718, <https://doi.org/10.1016/j.jcp.2009.12.017>.
- [38] D. WANG AND X.-P. WANG, *The iterative convolution-thresholding method (ICTM) for image segmentation*, Pattern Recognition, 130 (2022), p. 108794, <https://doi.org/10.1016/j.patcog.2022.108794>.